BIOCHEMISTRY
including biophysical chemistry & molecular biology
Article

Biochemistry **2009,** *48,* 9823–9830 9823
DOI: 10.1021/bi900258v

Characterization of the CHK1 Allosteric Inhibitor Binding Site

Darin Vanderpool,[‡] Ted O. Johnson,[§] Chen Ping,[∥] Simon Bergqvist,[‡] Gordon Alton,[‡] Soneprasith Phonephaly,[‡] Eugene Rui,[§] Chun Luo,[∥] Ya-Li Deng,[∥] Stephan Grant,[‡] Terri Quenzer,[∥] Steve Margosiak,[‡] James Register,[‡] Ed Brown,[‡] and Jacques Ermolieff *,[‡]

[‡]*Department of Biochemistry and Primary Screening and* [§]*Department of Chemistry and* [∥]*Department of Structural and Computational Biology, Pfizer, La Jolla, San Diego 92121*

Received February 16, 2009; Revised Manuscript Received August 25, 2009

ABSTRACT: Checkpoint kinase 1 (CHK1) is a key element in the DNA damage response pathway and plays a crucial role in the S-G_2-phase checkpoint. Inhibiting CHK1 is a therapeutic strategy involving abrogation of the G2/M mitotic checkpoint defense of tumor cells toward lethal damage induced by DNA-directed chemotherapeutic agents. To date, most CHK1 inhibition approaches have involved targeting the ATP site of this kinase. In this study, we provide crystallographic and kinetic characterization of two small molecule inhibitors that bind to an allosteric site in the proximity of the CHK1 substrate site. Analysis of kinetic and biophysical data has led to the conclusion that these small molecule allosteric site inhibitors of CHK1 are reversible and are neither ATP- nor peptide substrate-competitive. K_i values of 1.89 and 0.15 μM, respectively, have been determined for these compounds using a mixed inhibitor kinetic analysis. Cocrystal structures of the inhibitors bound to CHK1 reveal an allosteric site, unique to CHK1, located in the C-terminal domain and consisting of a shallow groove linked to a small hydrophobic pocket. The pocket displays induced fit characteristics in the presence of the two inhibitors. These findings establish the potential for the development of highly selective CHK1 inhibitors.

The duplication and partition of the genetic material throughout cell division is an intricate biological process that needs to be conducted with absolute fidelity. To ensure genome stability, each phase of the cell cycle is regulated by several checkpoint mechanisms, such as DNA damage or spindle assembly checkpoints. One of these mechanisms is represented by the ATM/ATR−CHK1/CHK2−CDC25−CDK axis (*1*, *2*). This pathway guards against mitotic catastrophe by ensuring that defects are detected and repaired at the G2/M checkpoint before the cell can progress to the next phase of the cell cycle. First-line therapies for cancer include radiation and chemotherapy and are designed to induce cell death by damaging the DNA material of cancerous cells. Because cancer cells utilize the checkpoints to facilitate repair of their DNA, the inhibition of CHK1[1] represents an attractive strategy for sensitizing cancer cells to cytotoxic chemotherapeutics. CHK1 is a protein kinase from the CAMKL kinase family, whose role is critical for the cell to enter mitosis. The transition to mitosis is delayed by the phosphorylation of Cdc25 phosphatase by CHK1. Upon phosphorylation, the activity of Cdc25 is inhibited by association with 14-3-3 proteins, which leads to an increase in the level of tyrosine phosphorylation of the CDK−cyclin complexes and blocks cell cycle progression. Only a few CHK1 inhibitors, UCN-01, XL-844, LY-2603618, AZD7762, and PF-00477736 (Figure 1), have reached clinical phase I or II (*2*−*5*); these five compounds inhibit CHK1 through binding in the ATP site, and all are competitive with ATP. The disadvantage associated with most of these ATP-competitive inhibitors resides in their difference in potency when tested in the cell and in the biochemical assay. This difference in potency is primarily due to the high concentration of ATP present in the cells (i.e., 1−10 mM). There is a growing interest in the development of non-ATP-competitive inhibitors for CHK1 and other protein kinases, to address these problems common to ATP site inhibitors. Currently, there are five non-ATP competitive kinase inhibitors in various clinical phases, against p38 MAP kinase, MEK1/2, and polo-like kinase I (*6*, *7*). Several other scientific studies also describe the development of such inhibitors against AKT (*8*).

This study reveals a unique allosteric site on CHK1 that has been characterized in the presence of two inhibitors from novel chemical series (i.e., a carbamate and a semicarbazide series). These findings are supported by kinetic, biophysical, and crystallography studies.

EXPERIMENTAL PROCEDURES

Reagents and General Assay Conditions. EDTA, Tris and Hepes buffer, DMSO, ATP, ADP, DTT, Surfactant 20 (P20), magnesium chloride, and Brij35 were purchased from Sigma-Aldrich (St. Louis, MO). Fluorescent syntide-2 (PLARTLSVAGLPGKK-5FAM) was synthesized in house at Pfizer and purchased from CPC Scientific Inc. (San Jose, CA). Fluorescent Cdc25 peptide (5FAM-KKKVSRSGLYRSPSMPENLNRPR) was purchased from Caliper LifeSciences (Hopkinton, MA). The syntheses of compounds **1**, **2**, and **3** (Figure 1) were conducted using protocols previously described in several published patents (*9*, *10*).

*To whom correspondence should be addressed: 10578 Science Center Dr., San Diego, CA 92121. Telephone: (858) 622-6093. Fax: (877) 481-3121. E-mail: Jacques.ermolieff@pfizer.com.

[1]Abbreviations: CHK1, checkpoint kinase 1; β-MeOH, β-mercaptoethanol; DMSO, dimethyl sulfoxide; DTT, dithiothreitol; EDTA, ethylenediaminetetraacetic acid; Hepes, 4-(2-hydroxyethyl)piperazine-1-ethanesulfonic acid; Tris, 2-amino-2-(hydroxymethyl)-1,3-propanediol; SPR, surface plasmon resonance; k_{on}, on-rate constant; k_{off}, off-rate constant; rmsd, root-mean-square deviation.

© 2009 American Chemical Society
Published on Web 09/10/2009

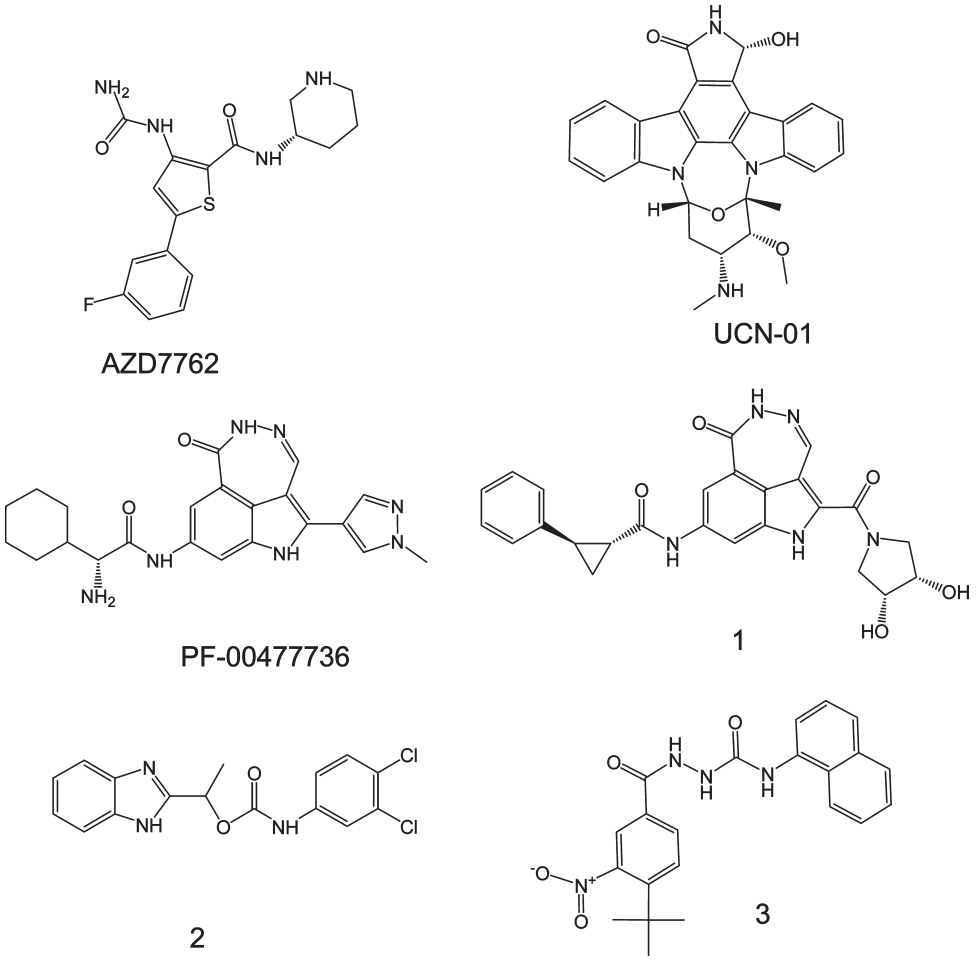

FIGURE 1: CHK1 compounds in clinical trials and described in this study. The structures of XL-844 and LY-2603618 remain undisclosed.

Kinetic studies were conducted in a 50 mM Hepes, 5 mM $MgCl_2$, 0.01% Brij35, 1 mM DTT assay buffer at pH 7.4 and room temperature (~22 °C) unless stated otherwise. All the concentrations of reagents used in this study are reported as final concentrations in the assay buffer. Enzyme concentrations correspond to the active site concentrations determined using a tight-binding inhibitor. Experimental data were generated at least in duplicate and were fitted using nonlinear regression analysis software, GraphPad Prism 5 (*11*).

Cloning, Protein Expression, and Purification of the CHK1 Kinase Domain. The nucleotide sequence of the wild-type human CHK1 kinase domain was amplified by PCR from a cDNA library and encodes amino acids 1−289. The amplified CHK1 kinase domain was cloned into the pFASTBAC vector to generate baculoviruses and for expression of the recombinant CHK1 protein in Sf21 cells. Cells were harvested 72 h after infection with baculoviruses.

The cell pellet was resuspended in lysis buffer containing 25 mM Tris-HCl (pH 7.5), 0.5 M NaCl, 5 mM β-MeOH, and 10 mM imidazole (pH 7.5) and later centrifuged at 125000*g* for 60 min. The supernatant was loaded into a Ni-NTA column, and the bound proteins were eluted with a linear gradient of imidazole (from 10 to 300 mM) in a buffer containing 25 mM Tris-HCl (pH 7.5), 0.5 M NaCl, 5 mM β-MeOH, and 5% glycerol. The eluted material (i.e., CHK1) was further purified using a Superdex 200 size exclusion column (Pharmacia).

Determination of the Apparent Michaelis−Menten Constants, K_m^{app} and k_{cat}^{app}. K_m^{app} and k_{cat}^{app} values for ATP were determined in the presence of 0.13 nM CHK1. The enzyme was incubated for 10 min in the assay buffer in the presence of 20 μM 5FAM syntide-2 in a 96-well V-bottom plate. The reaction was then initiated by addition of various concentrations of ATP. An aliquot of the assay mixture was then transferred to a low-volume 384-well black plate for determination of the relative amounts of substrate peptide and product phosphopeptide using a Caliper LC-3000 instrument (Caliper Life Science) from which the rate of turnover was calculated (micromolar per second). For the syntide-2 and Cdcd25 peptides, the apparent Michaelis−Menten constants were determined in a similar fashion by varying the amount of peptides in the presence of a fixed ATP concentration (500 and 100 μM for syntide-2 and Cdc25 peptides, respectively). The K_m^{app} for the peptide was determined using the following equation (see below) due to inhibition in the presence of excess substrate:

$$v = \frac{V_{max}}{1 + \frac{K_m^{app}}{[S]_o} + \frac{[S]_o}{K_i}} \quad (1)$$

where $[S]_o$ is the peptide concentration, K_i is the inhibition binding constant, and v and V_{max} are the rate and maximum rate of peptide phosphorylation in the presence of ATP, respectively.

The Caliper instrument was set up to collect aliquots from the assay mixture at regular intervals. For syntide-2, substrate and product were separated on the basis of charge using upstream and downstream voltages of −2700 and −500 V, respectively, and a screening pressure of −1.1 psi. For Cdc25, upstream and downstream voltages and pressure were set to −2250 V, −500 V,

Scheme 1

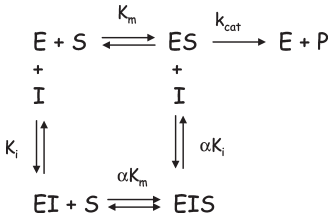

and −1.1 psi, respectively. K_m^{app} and k_{cat}^{app} values were calculated by measuring the amount of product generated with time.

CHK1 Inhibition. The inhibitors reported in this study bind to CHK1 according to a general mechanism illustrated in Scheme 1 where E, S, and I stand for enzyme, substrate, and inhibitor, respectively.

The K_i constant describing the inhibition of CHK1 is determined by fitting the experimental data to eq 2 (*12*):

$$V_i = V_o\left\{1 - \left[[E]_o + [I]_o + K_i^{app} - \sqrt{([E]_o + [I]_o + K_i^{app})^2 - 4[E]_o[I]_o}\right]/2[E]_o\right\} \quad (2)$$

where $[E]_o$ and $[I]_o$ are the active enzyme and inhibitor concentrations, respectively, K_i^{app} is the apparent inhibition binding constant, and V_i and V_o are the rates of syntide-2 phosphorylation in the presence and absence of inhibitor, respectively.

For noncompetitive inhibition and competitive inhibition, one substrate was fixed and K_i^{app} values were fitted using eqs 3 and 4, respectively, for K_i determination.

$$K_i^{app} = \frac{[A]_o + K_m^{app}}{\frac{K_m^{app}}{K_i} + \frac{[A]_o}{\alpha K_i}} \quad (3)$$

$$K_i^{app} = K_i + \frac{K_i}{K_m^{app}}[A]_o \quad (4)$$

When the peptide was fixed, A was the ATP concentration and α a parameter describing the effect of ATP concentration on the binding affinity of the inhibitor. CHK1 inhibition studies were conducted in a 96-well plate with enzyme (0.13 nM), syntide-2 (see the concentration reported in the legend of Figure 3), and various amounts of inhibitor. After preincubation for 15 min, the reaction was initiated via addition of ATP (see the concentrations reported in the legend of Figure 3) and quenched after 50 min via addition of 20 μL of an EDTA stock solution (i.e., 0.5 M) to each well. The assay mixture was treated as described in the previous section, and the product formation was measured using the Caliper LC-3000 instrument. The initial reaction velocity was determined by measuring the ratio of product and substrate in each well. Identical inhibition assay conditions were used when the peptide was varied instead of ATP.

Surface Plasmon Resonance Binding Assay. Surface plasmon resonance (SPR) biosensor binding studies were conducted using a Biacore 3000 instrument (GE Healthcare) at 20 °C in a 25 mM Hepes (pH 8.0), 150 mM NaCl, 5 mM $MgCl_2$, 0.005% P20, 0.5 mM DTT, 1% (v/v) DMSO running buffer. The CHK1 protein was immobilized on a CM5 chip by standard EDC/NHS amine coupling chemistry at 25 °C using a 1 μM solution of the protein with 200 μM ATP and 25 μM compound **3**, in 10 mM sodium acetate (pH 5.5). In a typical experiment, 180 μL injections of inhibitor were made at a flow rate of 50 μL/min and the dissociation time was monitored between 100 and 2800 s depending on the compound binding affinity. Data analysis was performed using Scrubber2 (BioLogic Software, Pty.). Compound injections were referenced to a blank surface and by a buffer blank. To determine the equilibrium dissociation constant (K_d), we plotted the observed response at equilibrium against the compound concentration and fit it to the following equation:

$$R = \frac{K_a[I]_o R_{max}}{K_a[I]_o + 1} \quad (5)$$

where R is the equilibrium response at a specific compound concentration, R_{max} is the response at a saturating compound concentration (i.e., $[I]_o$), and K_a is $1/K_d$. Kinetic constants were obtained from a fit to a kinetic binding model with mass transport, using Scrubber2.

Crystallization and Structure Determination. The cocrystallization was conducted by using hanging-drop vapor diffusion containing 2 μL of a 1:4 molar ratio of 8 mg/mL CHK1 protein solution to compound and 2 μL of a reservoir solution. Initial hit condition was obtained from Hampton Screen II (#37) with 10% (w/v) PEG 8K, 0.1 M Hepes (pH 7.5), and 8% (v/v) ethylene glycol in 25 mM Tris-HCl (pH 7.5), 0.5 M NaCl, 5% (v/v) glycerol, and 5 mM DTT protein buffer at 13 °C. The cocrystals of compounds **2** and **3** used for data collection were grown in 2.5−8% (w/v) PEG 8K, 0.1 M Hepes (pH 7.4), and 32−36% (v/v) ethylene glycol in 3−5 days at 13 °C. Data were collected in house at −175 °C using Mar345 and processed using HKL2000. The structure refinement was conducted using the published CHK1 structure (*13*) as the starting model. CNX was used for the entire course of refinement. Difference Fourier maps calculated with only protein model-derived phases showed well-defined electron densities for both compounds **2** and **3** (Figure 6). The refined inhibitors showed an average temperature factor consistent with that of surrounding protein residues. Data and refinement information are summarized in Table 1. Coordinates for the CHK1 complexes have been deposited in the Protein Data Bank as entries 3JVR (compound **2**) and 3JVS (compound **3**).

RESULTS

K_m^{app} and k_{cat}^{app} Determination. K_m^{app} and k_{cat}^{app} constants for ATP and peptide were determined from a standard Michaelis−Menten curve. For ATP, K_m^{app} and k_{cat}^{app} values of 38.5 ± 3.3 μM and 15.0 ± 0.4 s^{-1}, respectively, were determined in the presence of 20 μM syntide-2 (Figure 2a). For syntide-2, these values are 8.3 ± 1.2 μM and 16.7 ± 0.2 s^{-1}, respectively (Figure 2b), while a K_m^{app} of 4.2 ± 0.8 μM and a k_{cat}^{app} of 1.4 ± 0.1 s^{-1} were determined for Cdc25 (Figure 2c).

Enzyme−Inhibitor Complex Analysis. For compound **1**, observed K_i^{app} values increase with ATP concentration (Figure 3a) and decrease with peptide substrate (i.e., syntide-2) concentration (Figure 3b), suggesting that this compound behaves as a competitive inhibitor against ATP and as a mixed-type inhibitor against the peptide. Interestingly, the potency of compound **1** is enhanced as the concentration of peptide substrate increases, as illustrated in Figure 3b. We hypothesize that upon binding, the peptide substrate induces structural changes in the ATP-binding pocket and lowers the binding free energy of the inhibitor−enzyme complex.

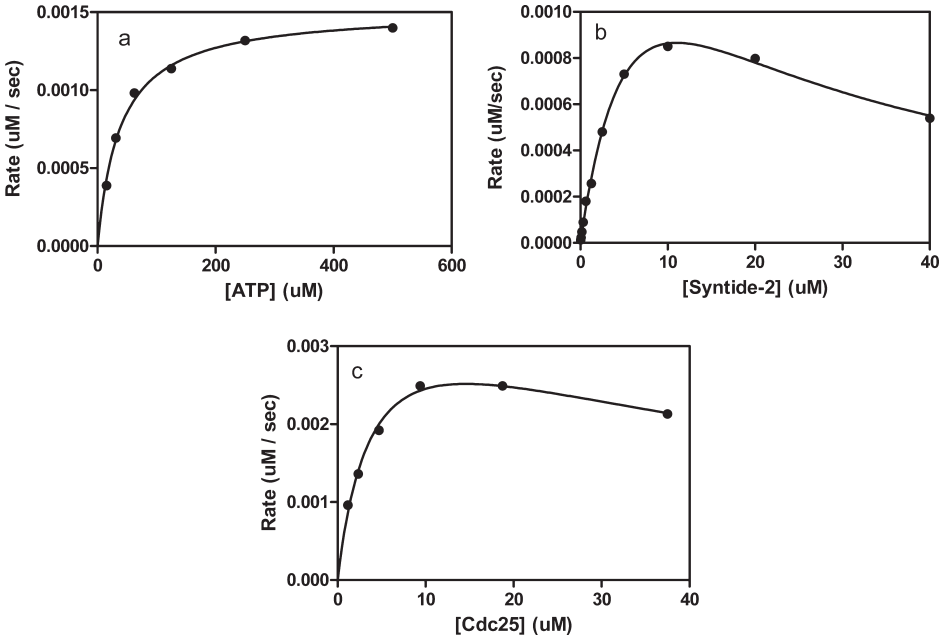

FIGURE 2: Kinetic study of the interaction of ATP and syntide-2 with CHK1. Kinetic data ($n = 2$) were generated by measuring the initial rate of product generated with time. A K_m^{app} value for ATP was determined using the Michaelis−Menten equation in the presence of 20 μM peptide ($R^2 = 0.99$) (a). For syntide-2 (b) and Cdc25 (c), the kinetic constants were determined as described in Experimental Procedures. Fixed ATP concentrations of 500 and 100 μM were used in the presence of syntide-2 ($R^2 = 0.99$) and Cdc25 ($R^2 = 0.99$), respectively.

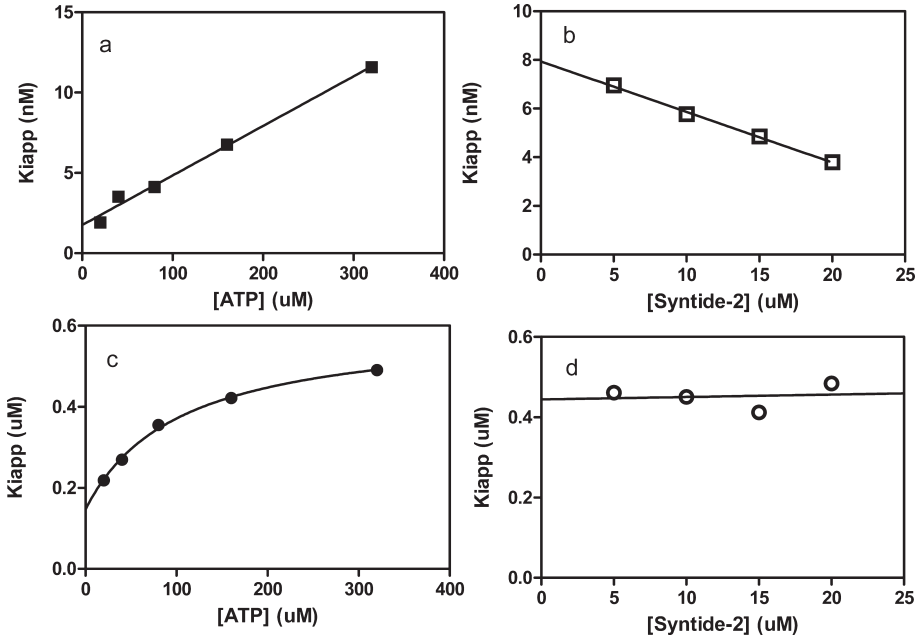

FIGURE 3: Inhibition of CHK1 in the presence of compounds **1** and **3**. The rates of substrate phosphorylation in the absence or presence of inhibitors were generated in duplicate. The K_i^{app} values for each compound were measured by varying the ATP and peptide concentrations in separate experiments. For compound **1**, K_i^{app} values increase linearly with ATP concentration (a) and decrease with syntide-2 concentration (b). Conversely, K_i^{app} values for compound **2** reach a plateau at a saturating concentration of ATP (c) or are not affected despite variation in the amount of peptide in the assay (d). A fixed ATP concentration of 160 μM and 20, 15, 10, and 5 μM syntide-2 were used to generate the data illustrated in panels b and d, while a fixed syntide-2 concentration of 5 μM and 320, 160, 80, 40, and 20 μM ATP were used to generate the data illustrated in panels a and c. Data in panels a and c have been fitted using eqs 4 and 3, respectively, with a calculated R^2 of 0.99 for both regression analyses. Data reported in panels b and d were fitted by using a simple linear regression analysis.

Results generated with compounds from the carbamate and semicarbazide series (compounds **2** and **3**) underline a different binding mode. As illustrated in panels c and d of Figure 3 (and Figure S1 of the Supporting Information), the presence of saturating concentrations of ATP or peptide substrates has a limited impact on the interaction of compound **3** with CHK1. From the plot of the experimental data reported in Figure 3c, a K_i value of 0.146 ± 0.003 μM was determined in the presence of syntide-2 using eq 3. In contrast with compound **1**, both compounds **2** and **3** display a mixed-type inhibition pattern in the presence of both nucleotide and peptide. K_i values generated during the course of our kinetic studies are reported in Table 2.

Biophysical Studies for Investigating Binding of ADP, ATP, and Inhibitor to CHK1. SPR biosensor technology was

used to directly measure binding of small molecules to immobilized CHK1 protein using a Biacore 3000 instrument. Because the SPR signal change is proportional to the molecular weight, small molecule binding studies can be challenging because of the small signal. However, it has been shown that the results of small molecule SPR experiments are highly reproducible over a wide range of binding affinities when care is taken with the experimental design and execution (*14*, *15*). Data for compound **1** were fit to a simple kinetic model with an observed K_d of 5.14 ± 0.38 nM [$k_{on} = (4.2 \pm 1.1) \times 10^5\ M^{-1}\ s^{-1}$, and $k_{off} = (2.1 \pm 0.4) \times 10^{-3}\ s^{-1}$ (Table 2 and Figure 4a)]. Competitive binding of compound **1** was confirmed by an apparent K_d approximately 7-fold higher in the presence of 240 μM ADP ($K_d = 36.0 \pm 0.6$ nM). Binding data for compound **3** with CHK1 in the absence of ADP or ATP were fit to a simple equilibrium model because of their lower binding affinity [$K_d = 0.29 \pm 0.07$ μM (Figure 4b)]. The observed binding affinity of compound **3** changed only 2-fold in the presence of an excess of ADP, consistent with noncompetitive binding with ATP [$K_d = 0.29 \pm 0.07$ μM in the absence of ADP vs $K_d = 0.66 \pm 0.22$ μM in the presence of 240 μM ADP (Table 2)]. ATP binding to CHK1 was characterized by an only 2-fold higher K_d relative to that of ADP [$K_d = 62 \pm 21$ and 27 ± 3.3 μM for ATP and ADP, respectively (Figure 4c, d)]. Lastly, binding of the syntide-2 peptide was investigated but could not be detected at peptide concentrations of up to 100 μM with or without ATP.

Table 1: Crystallographic Data and Refinement Statistics

compound	**2**	**3**
Crystal Data		
space group	$P2_1$	$P2_1$
unit cell dimensions *a*, *b*, *c* (Å)	44.8, 65.4, 57.9	44.8, 65.6, 57.9
unit cell dimensions α, β, γ (deg)	90, 93.67, 90	90, 93.73, 90
Diffraction Data[a]		
resolution range (Å)	40−1.76	50−1.90
no. of reflections measured	32001	26131
completeness (%)	96.0 (92.8)	98.0 (94.6)
redundancy of data	3.4 (3.3)	2.8 (2.7)
$\langle I/\sigma_I \rangle$	32 (4.3)	26 (4.6)
R_{sym} (%)[b]	4.1 (30.3)	4.9 (22.5)
Structure Refinement		
resolution range (Å)	40−1.76	40−1.90
no. of reflections used	30106	25032
R (%), R_{free} (%)[c]	20.2, 22.5	18.7, 21.5
no. of protein atoms	2106	2091
no. of solvent atoms	205	244
no. of compound atoms	23	30
rmsd for bond lengths (Å)	0.0042	0.0047
rmsd for bond angles (deg)	0.811	0.787
⟨*B* factor⟩, protein (Å^2)	26.3	26.7
⟨*B* factor⟩, ligand (Å^2)	24.5	37.9

[a]Values in parentheses refer to the highest-resolution shell. [b]$R_{sym} = \sum|\langle I \rangle - I| / \sum I$, where I is the measured intensity for reflections with indices *hkl*. [c]$R = 100 \times \sum|F_o - F_c| / \sum|F_o|$. R_{free} is the free R factor based on a random 5% of all data.

Structural Data Reveal a Unique CHK1 Allosteric Site. Crystallographic studies were undertaken to determine the mode of binding of inhibitors **2** and **3** to CHK1. Cocrystal structures generated with compounds **2** and **3** revealed a unique allosteric binding site located in the C-terminal domain adjacent to the αD helix (Figure 5). This site includes a hydrophobic pocket formed by the side chains of Phe93, Pro133, Leu206, and Ala200, along with side chains from the IEPDIG motif. This hydrophobic pocket has been proposed as the P-5 substrate binding site (*13*). The conserved PDIG motif limits the αD helix to a single turn, resulting in a shallow groove that wraps around the IEPDIG loop and merges with the hydrophobic pocket. Both compounds fill the pocket and a portion of the groove. Further analysis of these cocrystal structures reveals the detailed interactions between the inhibitors and CHK1. For compound **2**, the dichlorophenyl motif occupies the lipophilic P-5 pocket (see Figure 5 A,C). The phenyl side chain of Phe93 allows for some buried hydrophobic surface contact with the dichlorophenyl portion of the inhibitor. The NH group of the carbamate and the benzimidazole 1-NH group form hydrogen bonds with the backbone carbonyl groups of Phe93 and Asp94, respectively. The chiral methyl is in the *S*-configuration and is also making a hydrophobic interaction with the backbone and side chain of Asp94. The carbamate is binding in the shallow surface groove that wraps around the IEPDIG loop. The face of the benzimidazole group makes contact with the backbone and side chains of Glu97 and Pro98 (Figure 6).

Compound **3** binds in the same orientation as compound **2** but establishes two additional hydrogen bonds and makes more extensive hydrophobic surface contact. A water-mediated hydrogen bond is formed between the nitro oxygen of the inhibitor and the hydroxy group of the Tyr173 side chain. There is significant hydrophobic surface contact between the *tert*-butyl substituent and the backbone and side chains of Leu206 and Ala200 and the Glu205 backbone. Hydrogen bonding also exists between the 2-NH group of the hydrazide group and the carbonyl of Phe93, as well as between the 1-amino substituent of the naphthalene and the carbonyl of Ile96. The face of the naphthyl group interacts with the backbone and side chains of Glu97 and Pro98. The additional ligand−protein hydrogen bonds and increased hydrophobic surface contact of compound **3** may account for its increased binding affinity relative to that of compound **2**.

Table 2: Kinetic Parameters for ADP, ATP, and Inhibitors Determined with the Caliper and Biacore Technologies

	mechanism of inhibition		inhibition constants[d](Caliper)		equilibrium dissociation constants (SPR)
	ATP varied	peptide varied	K_i	α	K_d
ATP	n/a[a]	n/a[a]	n/a[a]	n/a[a]	61.0 ± 21.0 μM
ADP	C[b]	MT[c]	5.36 ± 0.92 μM	∞	27.2 ± 3.3 μM
compound **1**	C[b]	MT[c]	1.75 ± 0.27 nM	∞	5.14 ± 0.38 nM
compound **2**	MT[c]	MT[c]	1.89 ± 0.32 μM	2.1 ± 0.6	nd[e]
compound **3**	MT[c]	MT[c]	0.146 ± 0.003 μM	4.1 ± 0.2	0.29 ± 0.07 μM

[a]Not applicable. [b]Competitive inhibition mechanism. [c]Mixed-type inhibition mechanism. [d]These inhibition constants were determined when the ATP concentration was varied (see Figure 3a,c and Figure S3 of the Supporting Information). [e]Not determined.

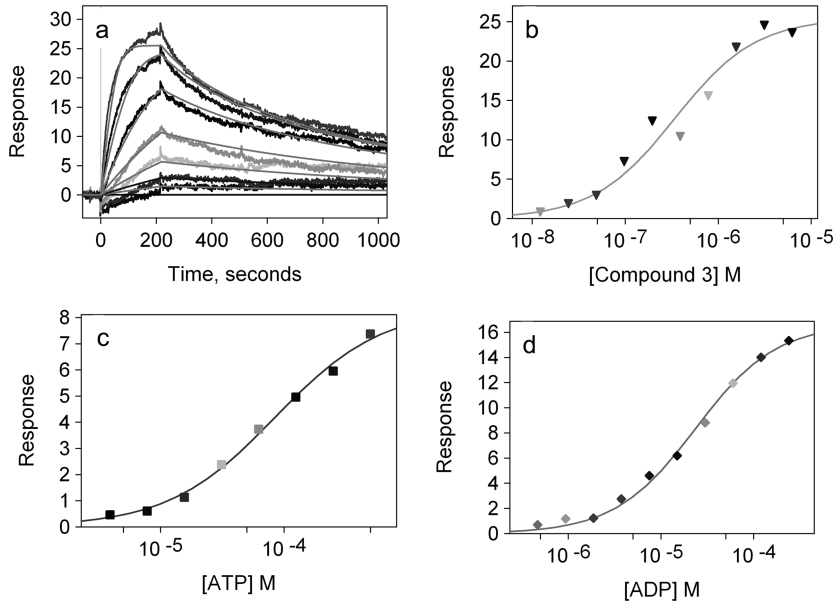

FIGURE 4: Surface plasmon resonance-based binding studies. As described in Experimental Procedures, the CHK1 enzyme is immobilized on a sensor chip and the binding of compounds **1**, **3**, ADP, and ATP to the enzyme was assessed by measuring the changes in the refractive index. The parameter K_d for compound **1** was determined from the individual constants k_{on} and k_{off} (a), while K_d values for compound **3** (b), ATP (c), and ADP (d) were determined by measuring the changes in the SPR response at equilibrium.

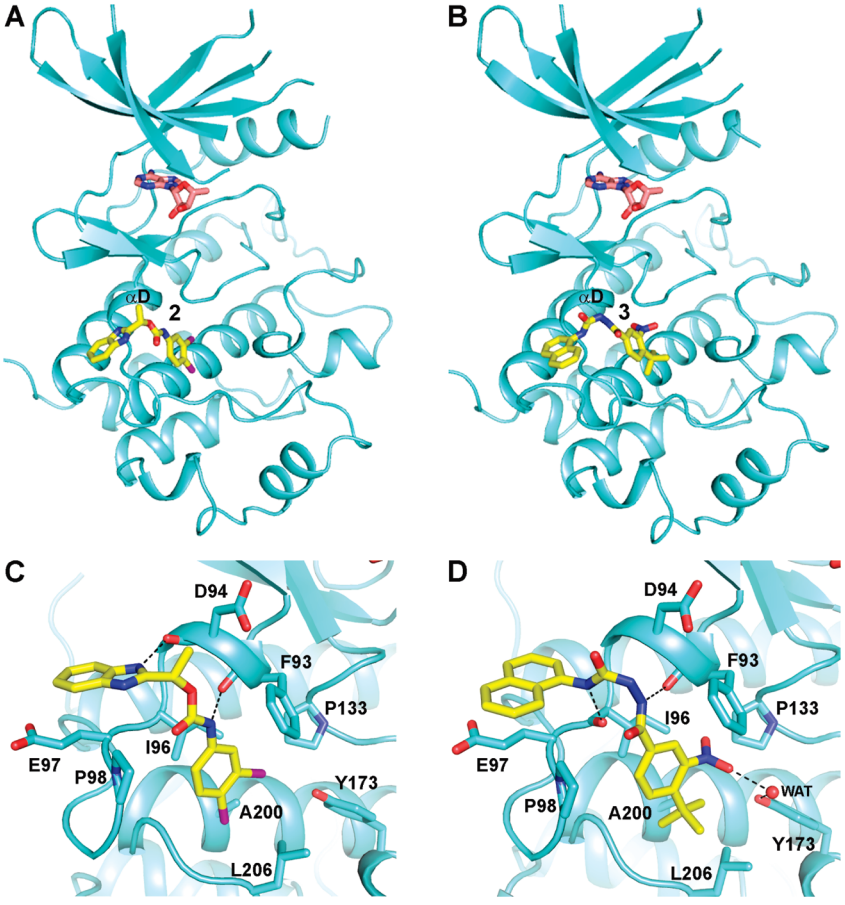

FIGURE 5: Cocrystal structures of CHK1 with inhibitors bound at the allosteric site located on the C-terminal domain adjacent to helix αD. An overall view of each complex is shown for (A) compound **2** and (B) compound **3**, with the inhibitor colored yellow and the expected position of the adenosine moiety colored pink, the latter based on an earlier structure of CHK1 with AMP-PNP (*13*). Closer views of each inhibitor are shown for (C) compound **2** and (D) compound **3**, featuring protein side chains that are important for the definition of the allosteric binding pocket.

DISCUSSION

The crystallographic studies reveal the existence of an allosteric site unique to CHK1 that was identified in the presence of carbamate and semicarbazide inhibitors, two new chemical classes of CHK1 inhibitors (see compounds **2** and **3** in Figure 1). The allosteric site is located near the peptide substrate

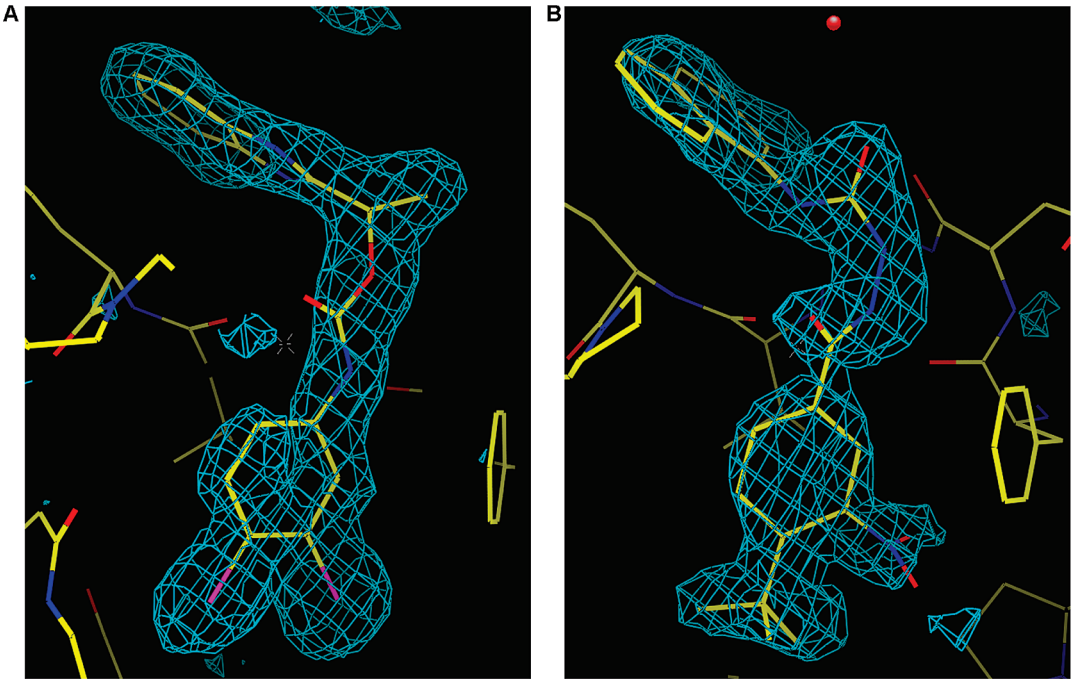

FIGURE 6: Electron density maps of compounds **2** (A) and **3** (B) bound to CHK1.

binding site and consists of a shallow groove and a small hydrophobic pocket delineated by the conserved IEPDIG motif and residues Phe93, Pro133, Leu206, and Ala200. Docked models of the natural substrate Cdc25c binding to CHK1 show that the terminal Leu of the Cdc25c substrate at the P-5 position interacts with the hydrophobic pocket of the allosteric site (*13*). Interestingly, the kinetic studies conducted here show that these inhibitors do not compete with the syntide-2 substrate, which also has a Leu residue at the P-5 position similar to the Cdc25 peptide (see Figure S1 of the Supporting Information). We suggest that both substrates can accommodate various orientations upon binding with the enzyme such that the terminal Leu residue can be positioned either in or out of the hydrophobic pocket. This hypothesis is supported by our Michaelis−Menten studies in which we observed inhibition of phosphorylation at high concentrations of peptides (Figure 2b,c). It is possible that in certain orientations of the peptide substrate in the enzyme binding site product formation does not always occur.

Our results showed that increasing concentrations of ATP in the assay can negatively impact the binding of these allosteric inhibitors to the enzyme. As illustrated in Figure 3c, the secondary plot of K_i^{app} versus ATP displays an upward hyperbolic curve reaching a plateau at saturating concentrations of ATP. The fitting of the data by eq 3 suggests that the potency of these allosteric inhibitors **2** and **3** decreased by factors of 2 and 4, respectively (see the α factor reported in Table 2). A likely explanation of these results is that the formation of the binary ATP−CHK1 complex induces structural changes in the allosteric site that interfere with the binding of these compounds. Approximate allosteric binding site volume calculations using the LIGSITE algorithm (*16*) were implemented in SuperStar (*17*). The crystal structure of the apoprotein allosteric pocket has an apparent binding site volume of 69.3 Å^3. Once binding with the ATP analogue, AMP-PNP (*13*), has taken place, the allosteric binding site volume decreases to 56.6 Å^3, which represents a decrease of 18% from that of the allosteric site in the apo structure. Cocrystal structures of CHK1 compounds **2** and **3** reveal subtle induced-fit binding effects that are reflected in the increased measured binding site volumes of 79.2 (14% increase) and 92.3 Å^3 (33% increase), respectively. No ternary complex between the CHK1−ATP complex and the allosteric inhibitors is available; however, we hypothesize that once ATP has bound, the surface area available for hydrophobic interaction with the allosteric inhibitor is reduced, leading to a decrease in the observed binding affinity. Lieser et al. (*18*) have previously shown how distal docking sites for the protein substrate can affect the affinity of the enzyme for ATP by modulating either the stability of the enzyme−ATP complex or the rate of phosphoryl transfer to the protein substrate. Whether these allosteric inhibitors directly affect the ability of the enzyme to bind ATP or alter the catalytic rate is not known. Nevertheless, the formation of the CHK1−allosteric inhibitor complex causes a decrease in the overall rate of product formation and thereby demonstrates a novel mode of inhibition of the rate of the CHK1 protein kinase reaction. On the basis of the model presented previously by Leiser et al., we also propose that these allosteric inhibitors can negatively impact 1) the binding of ATP to CHK1, 2) the binding of the substrate to the CHK1−ATP complex, and/or 3) the rate of transfer of the phosphate group to the substrate.

Recently, Converso et al. (*19*) reported the binding of a thioquinazoline chemical series to a region of CHK1 they define as an allosteric (non-ATP) site. This site features the same hydrophobic pocket as described above (the P-5 substrate site), into which the chlorophenyl portion of the thioquinazoline binds. However, the remainder of this inhibitor contacts a region of the enzyme that is a highly solvent exposed, relatively flat, and pointing away from the shallow groove adjacent to the αD helix that forms multiple interactions with compounds **2** and **3** (see Figure S2 of the Supporting Information). The larger amount of hydrophobic surface area of compound **3**, buried by the less solvent exposed hydrophobic regions of the protein, can possibly explain its higher observed activity (K_i = 0.146 μM), relative to the thioquinazoline series (optimum IC_{50} = 1.3 μM).

In conclusion, this study confirms the existence of an allosteric site on CHK1. This site has been kinetically and structurally characterized using molecules from a new structural class of CHK1 inhibitors. We have demonstrated that these molecules are potent inhibitors of CHK1 and bind in an allosteric site that shares a pocket with a site recently described by Converso et al. (*19*). The discovery of this novel allosteric site provides an opportunity to design more selective CHK1 inhibitors that are less compromised by ATP competition than typical ATP site inhibitors.

ACKNOWLEDGMENT

We are grateful to Dr. Bob Kumpf for his help in calculating the volume of the allosteric binding site of CHK1.

SUPPORTING INFORMATION AVAILABLE

K_i^{app} determination for compound **3** conducted in the presence of various concentrations of Cdc25 peptide (Figure S1), stereoview of the cocrystal structure for compound **2** (green) superimposed with inhibitor described by Converso et al. (yellow) (Figure S2), and ADP as a competitive inhibitor of CHK1 in the presence of ATP (Figure S3). This material is available free of charge via the Internet at http://pubs.acs.org.

REFERENCES

1. Chen, Y., and Poon, Y. C. R. (2008) The multiple checkpoint functions of CHK1 and CHK2 in maintenance of genome stability. *Front. Biosci.,* 5016–5029.
2. Bucher, N., and Britten, C. D. (2008) G2 checkpoint abrogation and checkpoint kinase-1 targeting in the treatment of cancer. *Br. J. Cancer 98*, 523–528.
3. Ashwell, S., and Zabludoff, S. (2008) DNA damage detection and repair pathways: Recent advances with inhibitors of checkpoint kinases in cancer therapy. *Clin. Cancer Res. 14*, 4032–4037.
4. Ashwell, S., Janetka, W. J., and Zabludoff, S. (2008) Keeping checkpoint kinases in line: New selective inhibitors in clinical trials. *Expert Opin. Invest. Drugs 17*, 1331–1340.
5. Blasina, A., Hallin, J., Chen, E., Arango, M. E., Kraynov, E., Register, J., Grant, S., Ninkovic, S., Chen, P., Nichols, T., O'Connor, P., and Anderes, K. (2008) Breaching the DNA damage checkpoint via PF-00477736, a novel small-molecule inhibitor of checkpoint kinase 1. *Mol. Cancer Ther. 8*, 2394–2404.
6. Kiselyov, A., Balakin, K. V., Tkachenko, S. E., and Savchuk, N. P. (2006) Recent progress in development of non-ATP competitive small-molecules inhibitors of protein kinases. *Mini-Rev. Med. Chem. 6*, 711–717.
7. Pargellis, C., Tong, L., Churchill, L., Cirillo, P. F., Gilmore, T., Graham, A. G., Grob, P. M., Hickey, E. R., Moss, N., Pav, S., and Regan, J. (2002) Inhibition of P38 MAP kinase by utilizing a novel allosteric binding site. *Nat. Struct. Biol. 9*, 268–272.
8. Lindsley, C. W., Barnett, S. F., Layton, M. E., and Bilodeau, M. T. (2008) The PI3K/Akt pathway: Recent progress in the development of ATP-competitive and allosteric Akt kinase inhibitors. *Current Cancer Drug Target 8*, 7–18.
9. Patent WO 2005/148643.
10. Patent WO 2004/063198.
11. *GraphPad Prism*, version 5.01, GraphPad Software Inc., San Diego.
12. Morrison, J. F. (1969) Kinetics of the reversible inhibition of enzyme-catalysed reactions by tight-binding inhibitors. *Biochim. Biophys. Acta 185*, 269–286.
13. Chen, P.; et al. (2000) The 1.7 Å crystal structure of human cell cycle checkpoint kinase CHK1: Implications for CHK1 regulation. *Cell 100*, 681–692.
14. Rich, R., Hoth, R. L., Geoghegan, F. K., Brown, A. T., LeMotte, K. P., Simons, P. S., Hensley, P., and Myszka, G. D. (2002) Kinetic analysis of estrogen receptor/ligand interactions. *Proc. Natl. Acad. Sci. U.S.A. 99*, 8562–8567.
15. Navtratilova, I.; et al. (2007) Thermodynamic benchmark study using Biacore technology, 2007. *Anal. Biochem. 364*, 67–77.
16. Hendlich, M., Rippmann, F., and Barnickel, G. (1997) LIGSITE: Automatic and efficient detection of potential small molecule-binding sites in proteins. *J. Mol. Graphics Modell. 15*, 359–363.
17. Verdonk, M. L., Cole, J. C., and Taylor, R. (1999) SuperStar: A knowledge-based approach for identifying interaction sites in proteins. *J. Mol. Biol. 289*, 1093–1108.
18. Lieser, A. S., Aubol, E. B., Wong, L., Jennings, A. P., and Adams, A. J. (2005) Coupling phosphoryl transfer and substrate interactions in protein kinases. *Biochim. Biophys. Acta 1754*, 191–199.
19. Converso, A.; et al. (2009) Development of thioquinazolinones, allosteric Chk1 kinase inhibitors. *Bioorg. Med. Chem. Lett. 19*, 1240–1244.